JOURNAL OF NEUROPHYSIOLOGY
Vol. 76, No. 5, November 1996. *Printed in U.S.A.*

Spike Train Encoding by Regular-Spiking Cells of the Visual Cortex

MATTEO CARANDINI, FERENC MECHLER, CHRISTOPHER S. LEONARD, AND J. ANTHONY MOVSHON
Center for Neural Science and Howard Hughes Medical Institute, New York University, New York 10003

SUMMARY AND CONCLUSIONS

1. To study the encoding of input currents into output spike trains by regular-spiking cells, we recorded intracellularly from slices of the guinea pig visual cortex while injecting step, sinusoidal, and broadband noise currents.

2. When measured with sinusoidal currents, the frequency tuning of the spike responses was markedly band-pass. The preferred frequency was between 8 and 30 Hz, and grew with stimulus amplitude and mean intensity.

3. Stimulation with broadband noise currents dramatically enhanced the gain of the spike responses at low and high frequencies, yielding an essentially flat frequency tuning between 0.1 and 130 Hz.

4. The averaged spike responses to sinusoidal currents exhibited two nonlinearities: rectification and spike synchronization. By contrast, no nonlinearity was evident in the averaged responses to broadband noise stimuli.

5. These properties of the spike responses were not present in the membrane potential responses. The latter were roughly linear, and their frequency tuning was low-pass and well fit by a single-compartment passive model of the cell membrane composed of a resistance and a capacitance in parallel (RC circuit).

6. To account for the spike responses, we used a "sandwich model" consisting of a low-pass linear filter (the RC circuit), a rectification nonlinearity, and a high-pass linear filter. The model is described by six parameters and predicts analog firing rates rather than discrete spikes. It provided satisfactory fits to the firing rate responses to steps, sinusoids, and broadband noise currents.

7. The properties of spike encoding are consistent with temporal nonlinearities of the visual responses in V1, such as the dependence of response frequency tuning and latency on stimulus contrast and bandwidth. We speculate that one of the roles of the high-frequency membrane potential fluctuations observed in vivo could be to amplify and linearize the responses to lower, stimulus-related frequencies.

INTRODUCTION

Since the fundamental work of Hodgkin and Huxley (1952), a very large body of data has become available on the mechanisms underlying the generation of spike trains. In cortical cells, in particular, spike train encoding was found to be controlled by an array of voltage- and calcium-dependent channels (see Gutnick and Crill 1995 for a recent review). Progress in modeling has made it possible to incorporate the physiological findings into detailed simulations of single cells or even whole networks (Bower and Beeman 1995; Koch and Segev 1989; McCormick and Huguenard 1992).

This extended and detailed knowledge is however not easily applied to the context of systems neuroscience, where attention is largely concentrated on factors such as the nature of the inputs to a network and the connectivity of different cell types. When modeling the responses of cells in the primary visual cortex, for example, one would like to devote the bulk of the model's parameters to factors such as the visual properties of subcortical inputs, the wiring of these inputs onto cortical cells, and the nature of intracortical feedback. Adding to these a detailed spike-encoding mechanism results in tens of additional free parameters, and in a heavy computational burden, which make it impossible to fit the model to actual data (see, e.g., Suarez et al. 1995). This suggests a need for a simple and robust model of the transformation of synaptic currents into spike trains by cortical cells.

In studies of the visual cortex, this transformation has been traditionally modeled with a simple stage that instantaneously converts somatic current or membrane potential into a continuous firing rate. Perhaps the simplest of these models is the rectification model (e.g., Movshon et al. 1978), which postulates that the firing rate is zero for membrane potentials below a threshold and grows linearly with the synaptic current above that threshold. Common variations of this model include functions with a smoother transition from rest (Heeger 1992b) and functions that saturate to a maximal firing rate, such as sigmoids. These models are all static (or memoryless) nonlinearities, i.e., ones whose output depends only on the present value of their input and not on past history.

Rectification and the other static models can be accurate in describing the steady-state responses of cortical cells, but fail to predict the time-varying responses. There is indeed a large body of literature pointing to a linear or bilinear steady-state relation between injected current and firing rate, once the current is above a threshold level (see Stafstrom et al. 1984b and references therein). In the primary visual cortex, in particular, the firing rate grows roughly linearly with injected current (Jagadeesh et al. 1992). When the stimuli are current steps, however, the firing rate of some cortical cells displays prominent adaptation (Connors et al. 1982). Firing rate thus depends not only on the injected current I, but also on time t. In addition, when the stimuli are current ramps, the resulting firing rate depends on the slope dI/dt of the ramp (Stafstrom et al. 1984b).

The aim of the present study is to gain a general understanding of the spike-encoding properties of cortical cells, and to provide a model of these properties that lies between the excessive simplicity of the static nonlinearity models and the complexity of the detailed biophysical descriptions. There are a number of models that could in principle capture the spike-encoding properties of cortical cells while being described by a limited number of free parameters. Among these models are variations on the integrate-and-fire scheme

(e.g., Getting 1989; Knight 1972), as well as sequences of basic signal-processing blocks such as linear filters and static nonlinearities (French and Korenberg 1989; Korenberg et al. 1989). The model that we advocate in the present study belongs to the latter category, and predicts smooth firing rates rather than spike trains.

We performed intracellular in vitro experiments on slices of the guinea pig visual cortex. We recorded from regular-spiking cells, which are known to be pyramidal or spiny stellate cells and to be excitatory (Connors and Gutnick 1990). We injected currents of various waveforms (sinusoids, broadband noise and steps) and analyzed the cells' membrane potential and spike train responses.

In the first part of this study we report on the spike train responses. We found that the responses to sinusoidal currents have very different properties from the responses to broadband noise currents. With sinusoidal currents the spike-encoding mechanism acts as a band-pass filter, and the averaged responses are very nonlinear. The nonlinearities are of two kinds: rectification, which refers to the absence of response in the negative portion of the stimulus, and spike synchronization, which refers to the recurrence of spikes at the same exact points in the stimulus cycle. In response to broadband noise, the cells are more responsive, and encode all the frequencies between 0.1 and 130 Hz equally well. In addition, the averaged responses are much more linear than with sinusoidal currents.

In the second part of this study we show that the above mentioned properties of the spike responses are not present in the underlying membrane potential traces. Indeed, a very large portion of the variance of the membrane potential responses can be captured by a simple single-compartment passive model of the cell, which is a linear low-pass filter.

In the final part of this study we propose a sandwich model that accounts quantitatively for the spike responses. It essentially consists of a static nonlinearity—the rectification stage—sandwiched between two linear filters (Korenberg et al. 1989; Victor et al. 1977). This model is an extension of the rectification model, and is similar to one proposed by French and Korenberg (1989) to describe the transformation of injected currents into spike trains by cockroach mechanoreceptors. The linear filter that precedes the rectification stage is low pass, and is determined by the passive properties of the cell membrane. The linear filter that follows the rectification stage is high pass, and presumably summarizes the effect of voltage- and calcium-dependent conductances. The whole model is described by six parameters.

In the DISCUSSION we compare our approach with those of other studies, we examine the possible role of the spike-encoding mechanism in shaping the visual responses of neurons in the primary visual cortex, and we speculate on the possible role of the high-frequency fluctuations observed in vivo by Jagadeesh et al. (1992).

Portions of this work have been presented as conference abstracts (Carandini et al. 1994, 1995).

METHODS

Preparation and maintenance

Brain slices were prepared from albino or pigmented guinea pigs (150–600 g) that were deeply anesthetized with pentobarbital sodium (35–70 mg/kg) and then decapitated. The skull was rapidly opened and the visual cortex was removed and placed in ice-cold Ringer solution. The cooled block was affixed to the stage of a vibratome with cyanoacrylate and 350-μm-thick slices were cut. Slices were individually incubated at room temperature in a Ringer solution continuously bubbled with 95% O_2-5% CO_2 until being placed into a recording chamber (between 1 and 12 h later) that was maintained at 22–33°C. The Ringer solution contained (in mM) 124 NaCl, 5 KCl, 1.2 NaH_2PO_4, 2.7 $CaCl_2$, 3 $MgSO_4$, 26 $NaHCO_3$, and 10 glucose.

Cells were impaled with glass micropipettes filled with 3 M KCl, having DC resistances of 70–150 MΩ. Intracellular recordings were performed with a current-clamp (Axon Instruments) recording amplifier utilizing capacitance neutralization. Current was injected through an active bridge circuit, allowing the voltage drop across the electrode resistance to be subtracted. The electrode was tested in the solution to make sure it did not introduce substantial rectification and other nonlinearities. Stimulus generation and data acquisition were all performed by computer through a CED 1401 Plus interface (Cambridge Electronic Design). Injection currents were sampled at 1–4 kHz; voltage traces were sampled at 4 kHz.

The recordings were obtained from neurons in the primary and secondary visual cortices (Choudhury 1978; Creel and Giolli 1972; Spatz et al. 1991; Wree et al. 1981). Neurons were identified as regular spiking if their response to current steps showed spike frequency adaptation, had no tendency to burst, and had a definite threshold for the generation of a single action potential (Connors and Gutnick 1990).

Stimuli

We used three types of stimuli. *1*) Steps, in which the current $I(t)$ stepped from I_0 to I_1 and back. *2*) Sinusoids: $I(t) = I_0 + I_1 \sin(2\pi f t)$. *3*) Broadband noise, obtained by adding eight incommensurate sinusoids: $I(t) = I_c \Sigma_{i=1}^{8} \sin(2\pi f_i t + \phi_i)$. The frequencies f_i were chosen so that their sums and differences would not coincide (Victor and Shapley 1980). The deterministic nature of this broadband signal makes it particularly useful for system identification purposes (Victor and Knight 1979).

Experiments contained a sequence of stimuli lasting 2–16 s each, separated by 4-s intervals during which no current was injected. The stimuli in each experiment were presented in random order to minimize the effect of slow drifts in the quality of the impalement. The order of the stimuli was recorded to assess the importance of such drifts. Each cell was tested with three core experiments.

1) A sequence of steps of different amplitude I_1.

2) A sequence of sinusoids of different frequency f and of different baseline intensity I_0 and/or amplitude I_1.

3) An experiment constituted by 16 stimuli: 8 broadband noise stimuli, in which the eight component sinusoids assumed different relative phases, and 8 sinusoid stimuli, in which the component sinusoids were presented alone. The values of the phases $\{\phi_i\}$, as well as the methods for computing the frequency tuning of the responses to the broadband stimuli, are described by Victor (1988). The amplitude of the component sinusoids was $I_1 = 0.25$–1 nA when presented alone, and $I_c = 0.075$–0.3 nA when presented with the others. Their ratio I_1/I_c was between 3 and 4. The root-mean-square intensity of the broadband stimuli was 70–95% that of the sinusoid stimuli. Two sets of frequencies f_i were used (in Hz): {0.933, 2, 4.133, 8.4, 16.933, 34, 68.133, 136.4} and {0.193, 0.452, 0.968, 2.0, 4.065, 8.193, 16.452, 32.968}. The frequencies in each set are integer multiples of a fundamental frequency, which is 0.133 Hz for the first set and 0.0643 Hz for the second set. Each

stimulus lasted one period of the fundamental frequency (7.5 or 15.5 s).

Data analysis

We analyzed two types of responses. The first was the raw membrane potential response $V(t)$, an analog signal. The second was the spike train response $S(t)$, a discrete signal that was computed from $V(t)$ off-line by detecting the downward crossings of $V(t)$ with a threshold around −10 mV. For mathematical analysis, the individual spikes were considered as Dirac delta functions, i.e., as infinitesimal intervals in which the firing rate was infinite. A spike train would thus have the form $S(t) = \Sigma_{j=1}^{N} \delta(t - t_j)$, where $\{t_j\}_{j=1}^{N}$ are the spike times. The Fourier transform of the spike train at a frequency f is $\hat{S}(f) = (2/T)\Sigma_{j=1}^{N} \exp(2\pi i f t_j)$, where T is the stimulus duration.

The sandwich model has three stages, defined respectively by *Eqs. 1, 2,* and *3* in the RESULTS section. Each stage has two free parameters. The parameters of the first stage (membrane resistance and capacitance) were estimated by fitting the transfer function of a circuit composed of a resistor and a capacitor in parallel (RC circuit, *Eq. 1*) to the first harmonics of the membrane potential responses. The remaining parameters, two for the rectifier (*Eq. 2*) and two for the high-pass linear filter (*Eq. 3*), were subsequently estimated by a minimization routine that searched for the minimum square difference between the model predictions and the spike trains. Both the model predictions and the spike trains were low-pass filtered, usually with a cutoff at 200 Hz, before their difference was computed.

RESULTS

We recorded from 26 cells in slices of the guinea pig visual cortex. Of these, nine satisfied our criteria for healthy impalements, were classified as regular spiking as described in the METHODS section, and were held long enough to be tested with the core experiments in our paradigm. The average resting potential of these cells was −70.2 ± 4.7 (SE) mV; their spike threshold was 31.1 ± 5.3 mV; and their spike height was 87.8 ± 6.2 mV. The average spike half-width was 1.1 ± 0.1 ms for the seven cells recorded at 33°C, and 2.5 and 3.4 ms, respectively, in the other two cells, which were recorded at 22°C.

To illustrate the relation between the responses to different stimuli, we chose to show data from the same cell in all figures. This cell (*19s2*) is typical of our sample, and the properties described in this study were extremely consistent across cells.

We recorded no spontaneous spikes when searching for cells, and we did not observe postsynaptic potentials in our intracellular recordings. This complete lack of spontaneous activity is a fundamental difference between our *in vitro* preparation and the normal *in vivo* conditions. Indeed, our voltage traces (e.g., Fig. 1) look very different from those obtained *in vivo* (e.g., Jagadeesh et al. 1992) in that they are entirely stimulus driven, and the only high-frequency fluctuation in membrane potential is given by the action potentials. As a consequence, the cells in this study should not be thought of as part of a network, but as single computational elements.

Spike train responses

SINUSOIDAL STIMULI. Figure 1 shows the responses of a cell to sinusoidal current injection. Figure 1, *B* shows the responses elicited with a modest stimulus amplitude (0.3 nA). Figure 1, *A* and *C* shows, respectively, the effect of doubling the amplitude of the stimulus and of introducing a positive baseline current (0.3 nA). In both conditions the cell fired more spikes. This is particularly clear for the 20-Hz stimuli (*bottom*), which did not elicit any spikes at low amplitude, and elicited many spikes at high amplitude or in the presence of a positive baseline current.

The spike-encoding mechanism of the cells exhibited a band-pass character. For frequencies below a certain cutoff frequency, increasing the stimulus frequency increased the number of spikes. Frequencies above the cutoff elicited no spikes. The value of the cutoff depended on stimulus amplitude and baseline intensity. A typical example of this behavior is shown in Fig. 2, which plots the amplitude and phase of the first-harmonic component of the spike responses as a function of stimulus frequency. The different curves correspond to different stimulus amplitudes (Fig. 2*A*) and baseline intensities (Fig. 2*B*). The responses to low-amplitude sinusoids in the absence of baseline injected currents are plotted in both *A* and *B* (*small* ●). In this condition the amplitude of the responses peaked at 5 Hz, and was zero above 15 Hz. Figure 2*A* shows that increasing the stimulus amplitude I_1 uncovered strong responses to the 15- and 20-Hz stimuli. Figure 2*B* shows that introducing a positive baseline current had a similar effect. This behavior was typical of all the cells we tested, irrespective of whether the spike responses were measured by their first harmonic or by the mean firing rate.

The curves fit to the phase data in Fig. 2 are the predictions of a simple model consisting of a delay with an arbitrary phase lead. These curves would be straight lines if plotted in a linear scale; the phase versus frequency plot of the output of a delay is a line whose negative slope is equal to the duration of the delay. We call the intercept of the fitted line with the ordinate the phase lead of the system, and the negative slope of the line the integration time of the system. The phase lead of the spike-encoding mechanism was positive, indicating that the spike responses to low-frequency sinusoids were concentrated on the rising phases of the stimulus. This phase lead increased with stimulus amplitude or baseline intensity. The integration time of the spike-encoding mechanism did not vary with the amplitude of the sinusoidal currents. It decreased with their baseline intensity, a phenomenon that we further examine in the context of the responses to broadband noise.

BROADBAND NOISE STIMULI. The frequency tuning of the firing rate measured with broadband noise was very different from that measured with single sinusoids. The cells were more responsive both to the low and to the high frequencies when they were part of a broadband stimulus than when they appeared as a single sinusoid. A typical example of this behavior is shown in Fig. 3. Although the frequency tuning of the firing rate gain measured with single sinusoids was markedly band-pass (●), that measured with broadband stimuli was flat or mildly high pass (*gray* ○). In other words, all the frequencies present in the boadband stimuli were represented in the spike train, with no sign of attenuation.

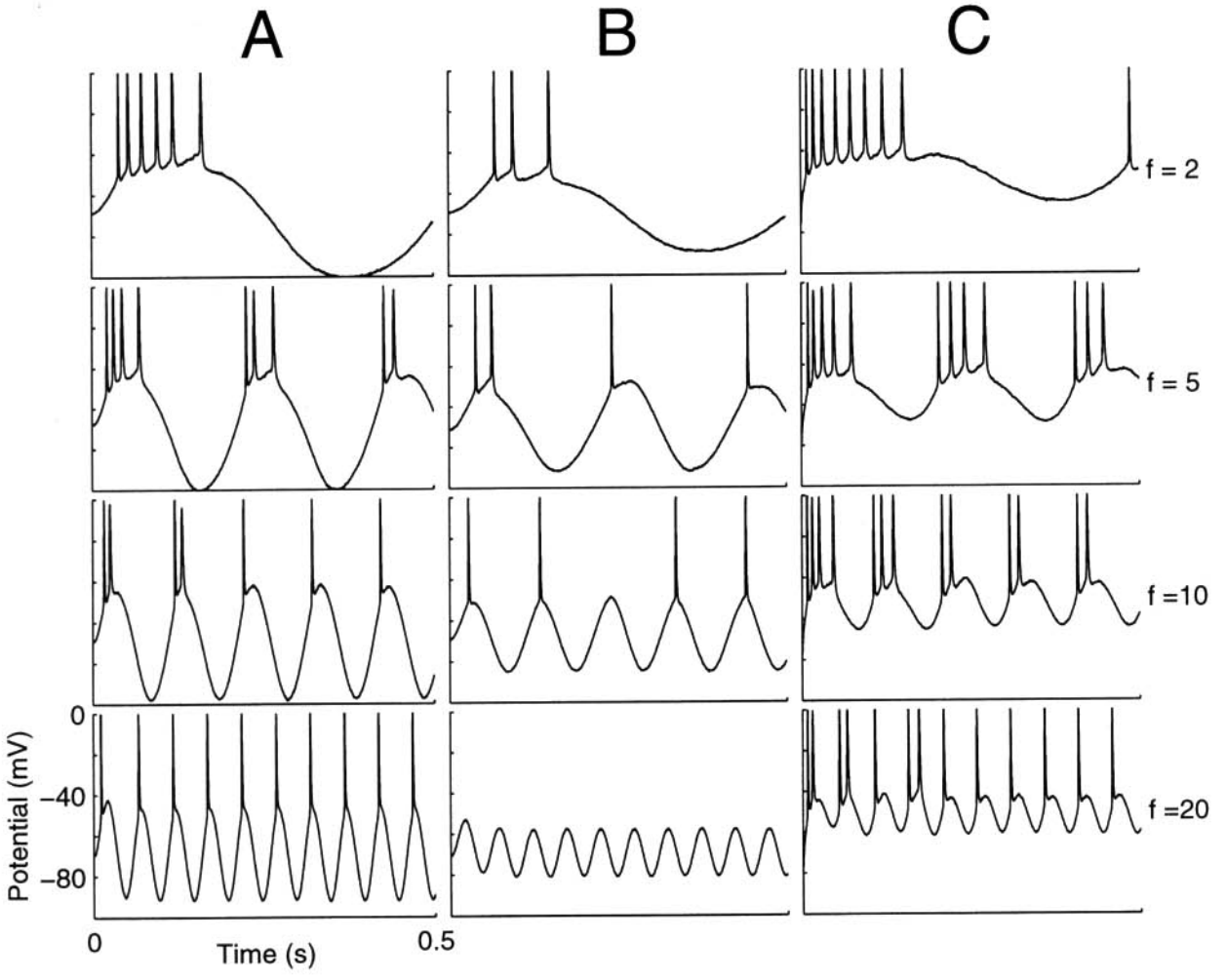

FIG. 1. Responses to sinusoidal current injections. Rows correspond to different frequencies of stimulation (f = 2, 5, 10, and 20 Hz). The modulation amplitude was I_1 = = 0.6 nA in *A* and 0.3 nA in *B* and *C*. In *C*, the stimulus had a positive baseline intensity I_0 = 0.3 nA (the baseline intensities in *A* and *B* were 0). Spikes are truncated at 0 mV. *Cell 19s2, experiment 5.*

Response phase is another aspect in which the spike train responses to broadband noise differed from the responses to single sinusoids. The slope of the phase versus frequency lines was steeper for sinusoids than for broadband noise, indicating a decrease in the integration time of the spike-encoding mechanism. The responses to broadband noise were advanced by ~10 ms with respect to sinusoids. Also, the phase lead decreased, from ~45° for sinusoids to ~10° for broadband noise. This means that whereas with single low-frequency sinusoids the spikes were concentrated on the rising phases of the stimulus, when these sinusoids were part of a broadband stimulus the responses were concentrated on the peak of the stimulus cycle.

The results of the broadband noise experiments were nearly identical in all the cells of our sample. This is made clear in Fig. 4. Figure 4, *top,* shows the responsivity of the cells as measured with sinusoids (*A*) and with broadband noise (*B*), as a percentage of the maximal responsivity to broadband noise. At frequencies <8 Hz, the responsivity of all cells was mildly enhanced by the broadband stimulation. Between 8 and 20 Hz, the responsivity was essentially the same with broadband noise and with sinusoids. At frequencies >20 Hz, the responsivity was dramatically enhanced by the broadband stimulus. Figure 4*C* shows how for all cells the integration time was shorter when measured with broadband noise than when measured with sinusoids: the mean integration times were 3 ± 1 ms and 14 ± 5 ms, respectively. The phase lead also changed substantially in the two conditions, from 28 ± 7° to 6 ± 3° (Fig. 4*D*).

NONLINEARITIES. If spike train encoding were a linear system, the spike density in response to a sinusoidal current injection would modulate sinusoidally. Figure 5*A* shows that this was far from being the case. The period histograms of the spike responses to sinusoidal current injection displayed two kinds of nonlinearity (Ascoli et al. 1974; French et al. 1972). The first nonlinearity was response rectification: there are spikes only when the sinusoidal currents are positive. This nonlinearity is to be expected in visual cortical cells, because these cells usually show no spike activity at rest and firing rates cannot be negative. The second nonlinearity is spike synchronization, which means that spikes tend to occur at particular times in the stimulus cycle. This results in sharp peaks in the spike histograms.

These nonlinearities are not present in the responses to

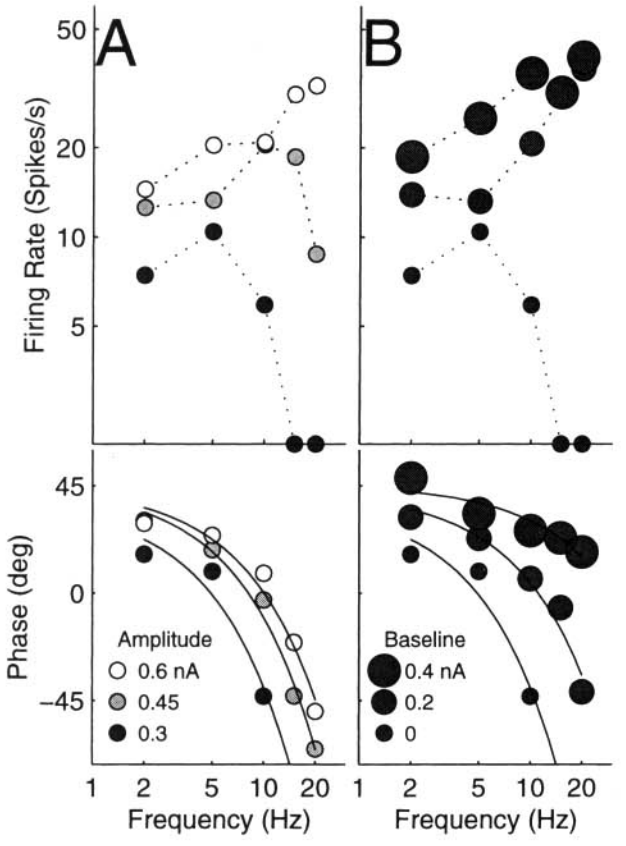

FIG. 2. Frequency tuning of the firing rate responses to sinusoidal currents for different stimulus amplitudes (*A*) and baseline intensities (*B*). *Top*: amplitudes of the responses. *Bottom*: phases. The cell acted as a bandpass filter whose best frequency depended on the stimulus amplitude and baseline intensity. Firing rates were measured by computing the first harmonic components of the spike trains. Some of the responses appear in Fig. 1. The continuous curves fitting the phase data are the predictions of a delay. They would become lines if they were plotted in linear scale. *Cell 19s2, experiment 5.*

broadband noise. An example of this is shown in Fig. 5*B*, in which are plotted the period histograms corresponding to the eight frequencies present in the broadband stimulus. The stimulus was proportional to the sum of the sinusoidal currents of Fig. 5*A*. The responses to the broadband stimuli were much more sinusoidal than the responses to the sinusoids (Fig. 5*A*), and indeed were well described by their first harmonic. This effect is known as linearization by noise (Spekreijse and Oosting 1970).

The linearizing effect of broadband noise cannot be judged exclusively from period histograms such as those shown in Fig. 5. By construction, period histograms average out any frequency components that are not multiples of the fundamental frequency of the histogram. The responses to broadband stimuli could still be very nonlinear and have power at frequencies that are not multiples of the eight input frequencies; this nonlinearity would not appear in Fig. 5*B*. In addition, histogramming is a form of smoothing, which hides the high-frequency components of the responses. For example, the third frequency in Fig. 5 (0.965 Hz) is 5 times the first frequency (0.193 Hz). The strong component of the responses at the higher frequency (*B, 3rd panel*) does not, however, appear in the period histogram of the lower frequency (*B, 1st panel*), because the histograms contain eight bars and are thus only able to reveal harmonics below the fourth.

To assess more precisely the degree to which broadband noise linearized the spike responses, we analyzed their spectral composition. The responses of a nonlinear cell would contain sinusoids of frequencies not present in the stimulus. These additional frequencies would be expected to include the sums and/or differences of some of the frequencies present in the stimulus (Victor and Shapley 1980). For a single sinusoid stimulus, these correspond to the zeroth and second harmonics. Consistent with the nonlinearity observed in the period histograms, the responses to sinusoidal currents showed substantial power at the second harmonic: on average the peak power of the first-harmonic responses to sinusoids was only 1.2 ± 0.3 times larger than that of the second-harmonic responses. The broadband stimuli contained eight frequencies, yielding 64 possible sums and differences of

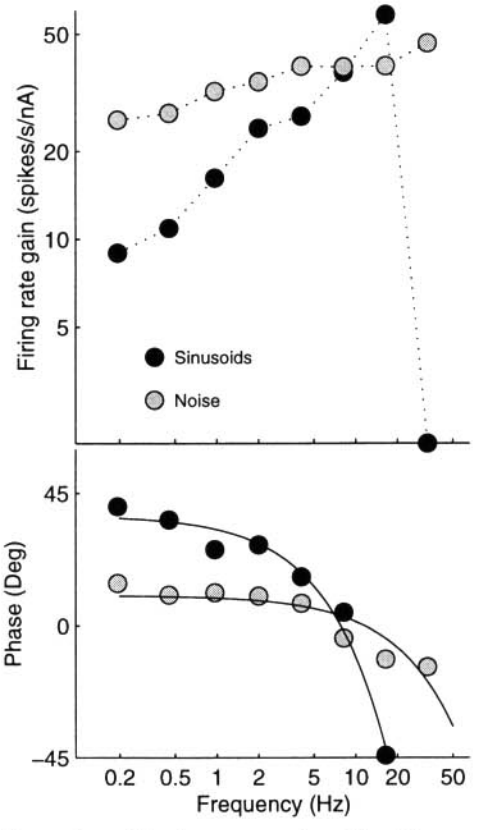

FIG. 3. Comparison of the frequency tuning of the firing rate responses to sinusoids and to broadband noise. *Top*: gain of the responses. *Bottom*: phase. Gain was measured by computing the first harmonic of the spike trains at a given component frequency and dividing the result by the intensity of that component in the stimulus. Stimulation with broadband noise enhanced the cell's responsivity to the low frequencies and uncovered strong responses to 33 Hz. The broadband noise was the sum of 8 sinusoids whose amplitude was 0.135 nA. When injected alone, the intensity of the sinusoids was 0.45 nA. The continuous curves fitting the phase data are the predictions of a delay and would become lines if they were plotted in linear scale. Their negative slope is a measure of the delay of the responses ("integration time"). Their intercept with the 0-frequency axis is a measure of the phase by which they lead the current injections ("phase lead"). *Cell 19s2, experiment 4.*

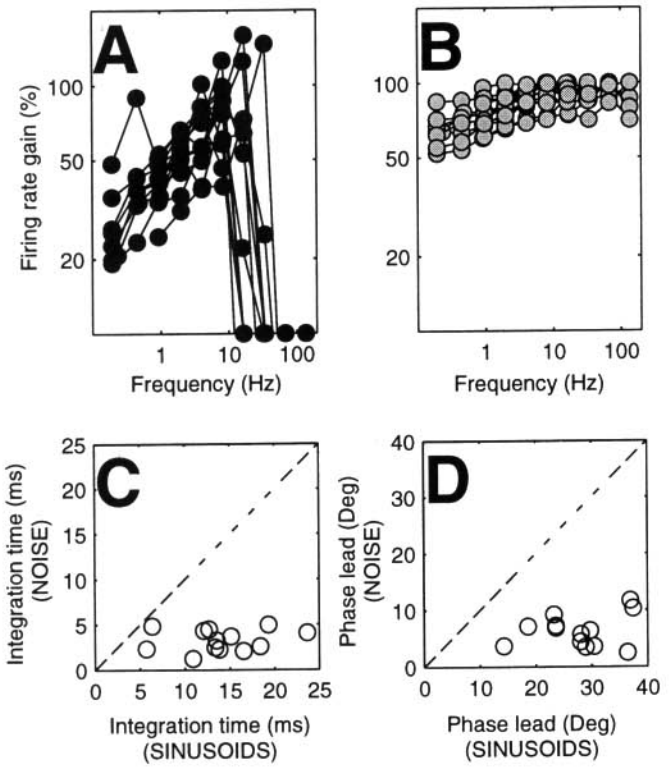

FIG. 4. Summary of the data obtained with sinusoid and broadband noise currents in all cells in our sample. *Top*: frequency tuning of the responses as measured with sinusoidal currents (*A*) and with broadband noise currents (*B*). To facilitate comparison, each cell's responses were normalized by its maximal response to the broadband stimuli. The responsivity of every cell was enhanced by the broadband stimuli, except in the range between 10 and 20 Hz, where on average it remained constant. *Bottom*: differences in the time course of the responses to sinusoids and broadband noise. Integration time and phase lead were obtained from the responses of each cell to sinusoids and broadband noise, by fitting the phase vs. frequency data with lines, as in Fig. 3, *bottom*. Both the integration time (*C*) and the phase lead (*D*) were shorter in the responses to broadband noise than in the responses to sinusoids.

frequencies. The Fourier component of the responses at these sum and difference frequencies is called the "second-order kernel" of the responses (Victor et al. 1977), and is a measurement to which we will return when evaluating the predictions of the sandwich model. We found that on average the peak power of the responses at the stimulus frequencies was 2.4 ± 0.8 times larger than the peak power of the second order kernel, confirming the linearizing effects of broadband noise on the spike responses.

Membrane potential responses

The simplest possible model of the transformation of injected currents into membrane potentials is a single-compartment passive model of the membrane composed of a capacitance and a resistance in parallel (RC model). There are some indications that this model may be at least partially successful in describing the subthreshold responses of cortical neurons. For example, Stafstrom et al. (1984a) reported an approximately linear current-voltage relation for the membrane potentials of cortical cells below threshold. The passive model is, however, clearly incomplete above threshold, where the membrane potential responses exhibit a variety of nonlinearities, which of course include the spikes themselves. These phenomena have been extensively studied, and a large body of knowledge is now available that describes the passive and active properties of these cells (Connors and Gutnick 1990; Connors et al. 1982; Douglas and Martin 1990; Gutfreund et al. 1995; Lorenzon and Foehring 1992; McCormick et al. 1985; Schwindt et al. 1988a–c; Stafstrom et al. 1984a–c).

We were interested in modeling the transformation of injected currents into membrane potentials with as few free parameters as possible, so that we could use such a model as the first stage of a model of the spike train responses to injected currents. Being described by just two parameters, the RC model of the membrane was an ideal candidate for this first stage. We therefore set out to measure the discrepancy between its output and the membrane potential responses of our cells. We were somewhat surprised to find that in most respects this simple linear model provided an acceptable first approximation to the membrane potential responses, even above threshold.

SINUSOIDAL STIMULI. The membrane potential responses of our cells were largely consistent with the output of a linear filter. This substantial linearity can be assessed by observing the degree to which the responses to sinusoidal currents were sinusoidal. Formally, this was done by investigating their spectral composition and comparing the size of their first-harmonic component with that of all the other components. Figure 6 illustrates this analysis. Figure 6*A* shows one period of the response of a cell to a sinusoidal current. Figure 6*B* shows the decomposition of the response into a first-harmonic component and a residual response, which is essentially constituted by the action potentials. Figure 6*C* plots the power of the different frequencies in the response. The spikes are fast events that contribute very little power: their presence does not strongly affect the spectral composition of the responses. The first harmonic clearly dominated the response. The power of the first harmonic was between 9 and 141 times the power of the second harmonic. The total harmonic distortion—the total power at the harmonics higher than the first—was 3.8% (median) of the power at the first harmonic.

We performed the same data analysis on the membrane potential responses as on the spike train responses to characterize the relation between the two types of response. The frequency response of the membrane potential responses, shown in Fig. 7, was very different from that of the firing rate (Fig. 2). The membrane clearly acted as a low-pass filter, with a corner frequency around 10 Hz.

The curves shown in the figure are the predictions of the RC model, the single-compartment passive model of the membrane. The frequency tuning predicted by the RC model is

$$\hat{V}(f) = \hat{I}(f)R/(1 + 2\pi i f\tau) \qquad (1)$$

where $\hat{V}$ and $\hat{I}$ are the Fourier transforms of the membrane potential V and of the stimulus intensity I. The variable f is the frequency of the stimulus, and the parameters R and τ are the membrane resistance and time constant. The model

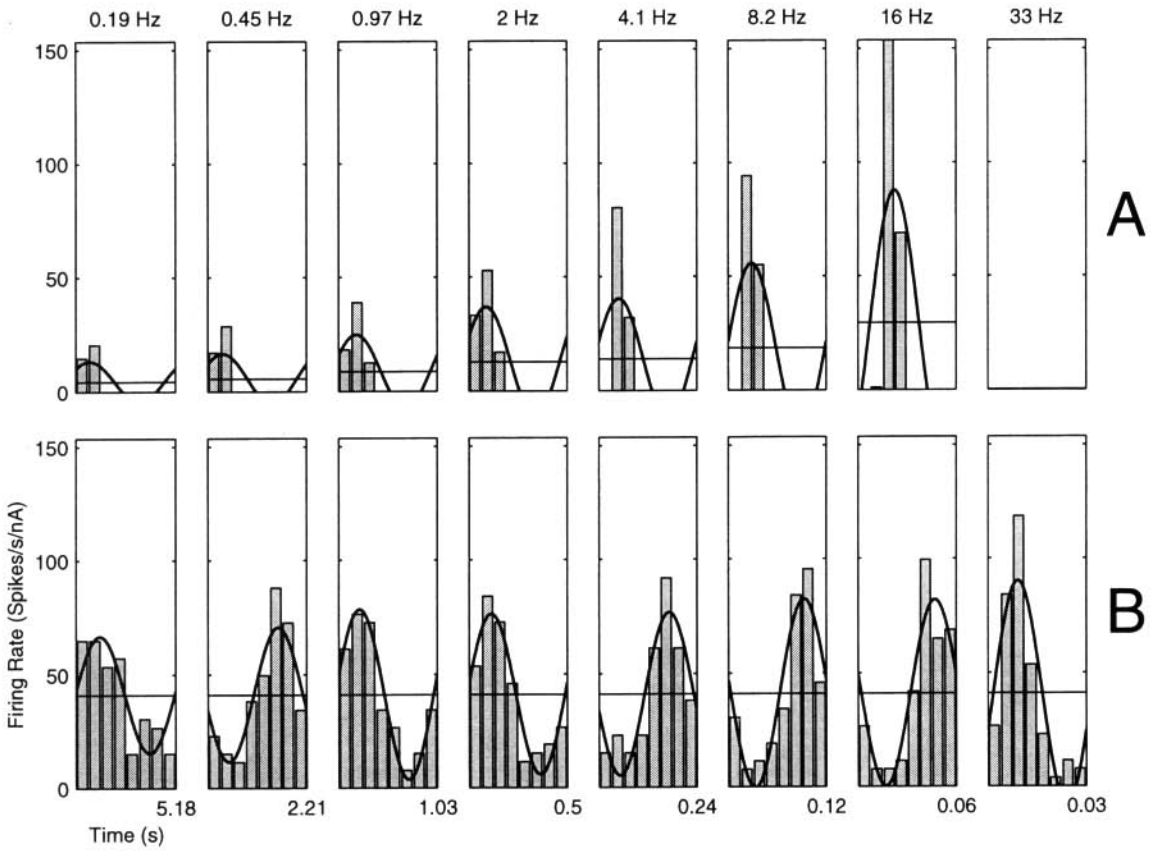

FIG. 5. Period histograms of the spike responses to sinusoids (*A*) and to broadband noise (*B*). Horizontal lines: mean firing rates. Sinusoidal curves: first harmonic of the responses. *A*: responses to 8 different sinusoids. The amplitude of the sinusoids was $I_1 = 0.45$ nA. *B*: response to broadband noise obtained by adding the 8 sinusoids. The amplitude of each sinusoid was $I_c = 0.135$ nA. Each panel shows the spike rate over the period of one of the component sinusoids. The 8 panels originate from the same spike train, and differ only in the period used to average the responses. The sinusoid histograms show 2 nonlinearities: "rectification" (the spikes do not encode the negative portions of the signal) and "spike synchronization" (the cell tends to spike at particular stimulus phases). In the presence of broadband noise both nonlinearities disappear: histograms are much more sinusoidal ("linearization by noise"). *Cell 19s2, experiment 4.*

was fit to the amplitude and phase of all the responses shown in Fig. 7, and all the curves that appear in the figure were determined by the same two parameters, R and τ. The fits of the RC model were generally satisfactory. On average, the fits accounted for 80% of the variance of the first-harmonic data. For comparison, the fit in Fig. 7 captures 87% of the variance. The parameters of the fits to all the cells in our sample are listed in Table 1.

Figure 7 also illustrates some deviations from perfect linearity in the membrane potential responses. Indeed, if the cells were perfectly linear, changing the baseline intensity of the stimuli would not affect the amplitude of their first-harmonic responses. In that case, the data points that have the same gray level (stimulus amplitude) but different sizes (baseline intensities) would coincide. Instead, Fig. 7*B* shows that the frequency tuning did show a mild dependence on the baseline intensity. In addition, if the cells were perfectly linear, neither the amplitude nor the baseline intensity of the stimuli would affect the phase of the responses. Instead, the phase data in the figure do show a dependence on stimulus amplitude and baseline intensity.

For some stimulus conditions the membrane potential responses of some cells displayed mildly band pass transfer functions, peaking at 4–8 Hz. An example of such a transfer function is shown in Fig. 8 (gray symbols). In this case, the amplitude of the responses was higher at 8 Hz than at lower frequencies, and the phases led the predictions of the RC model. This band-pass behavior was overall very mild, and was consistent with the recent results of Gutfreund et al. (1995), who in a similar preparation found subthreshold oscillations and resonant frequencies in the 3- to 20-Hz range. Similar resonant behaviors have been observed in other types of cortical cells (Llinàs et al. 1991; Silva et al. 1991). Accounting for this aspect of the frequency tuning of the membrane potential would require a more sophisticated model than a single RC circuit, for example one that included voltage-dependent conductances that would act as phenomenological inductances (Cole and Baker 1941; Gutfreund et al. 1995; Koch 1984).

BROADBAND NOISE STIMULI. Unlike the spike train responses, the membrane potential responses to broadband currents were closely predictable from the responses to sinusoids. This is illustrated in Fig. 8: the membrane potential had essentially the same frequency tuning whether it was measured with sinusoids (●) or with broadband noise (*gray* ○). This behavior is another piece of evidence for the partial linearity of the membrane potential responses. Consistent

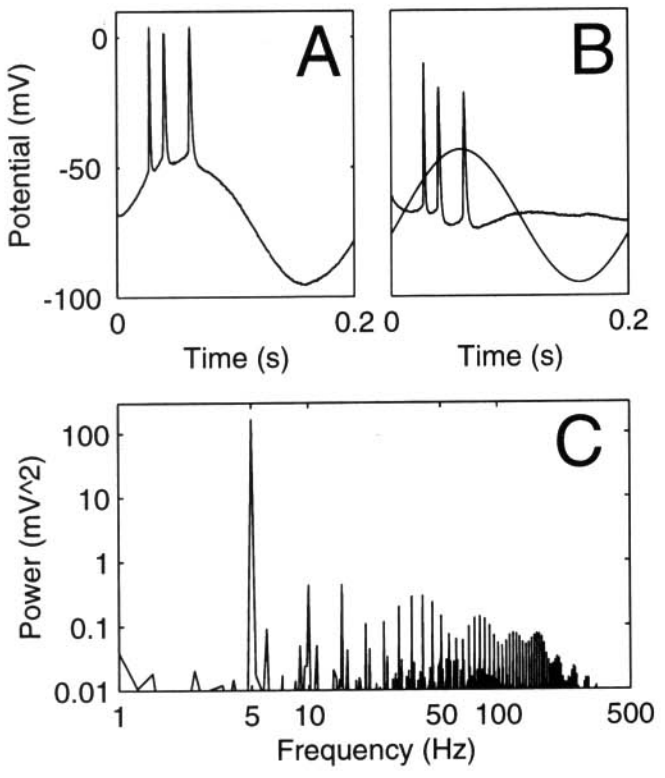

FIG. 6. Predominance of the first harmonic of the membrane potential response to sinusoidal current. *A*: 1st period of a response to sinusoidal current injection at a frequency $f = 5$ Hz. The baseline intensity was $I_0 = 0$ and the amplitude was $I_1 = 0.45$ nA. *B*: decomposition of the response into first harmonic and residual (actual response minus first harmonic). Besides the spikes, the residual traces are substantially flat. *C*: squared amplitude of the Fourier transform of the response. The first harmonic ($f = 5$ Hz) is by far the largest frequency component in the response. *Cell 19s2, experiment 5.*

with this linearity, most of the power of the membrane potential responses to the broadband stimuli was concentrated at the eight frequencies that composed the stimuli. The peak power of the responses at the component frequencies was between 11 and 426 (mean: 133) times larger than the peak power of the responses at the sums and differences of the component frequencies.

To ascertain whether the equivalence of the membrane potential responses to sinusoids and to broadband noise was shared by all our cells, we fit the first-harmonic responses to broadband noise and sinusoids independently with the use of *Eq. 1* and compared the parameters obtained in the two conditions. The result is illustrated in Fig. 9: neither the resistance nor the time constant changed substantially between the two stimulus conditions. In some cells, however, the sinusoid measurements appeared more erratic, and the quality of the fits achieved by *Eq. 1* was lower than that of the fits to the broadband noise measurements. On average, the root-mean-square error in the fits to the broadband noise measurements was 72% of the root-mean-square error in the fits to the sinusoid measurements. This occasional discrepancy may be due to the higher intensities used in the sinusoid stimuli, which may have activated strong active conductances.

Sandwich model

To account for the transformation of injected currents into firing rates, we have used a simple "sandwich" model. Sandwich models are composed of a static nonlinearity sandwiched between two linear filters, and have been used to model a variety of neural systems (French and Korenberg 1989; Korenberg et al. 1989; Victor 1988; Victor et al. 1977). Figure 10*A* illustrates the structure of the model.

The first stage of the model is a low-pass linear filter, the single-compartment passive model of the membrane. Its input is the injected current $I(t)$ and its output is a linear prediction of the membrane potential $V(t)$. This stage is described (in the frequency domain) by *Eq. 1*, which is fully determined by two parameters: the membrane resistance R and the time constant τ.

The second stage is a static nonlinearity: a rectifier with threshold V_T. Its output m is given by

$$m(t) = G \max [0, V(t) - V_T] \quad (2)$$

This stage has two free parameters: the threshold V_T (in mV), and the gain G (in spikes $\cdot s^{-1} \cdot mV^{-1}$).

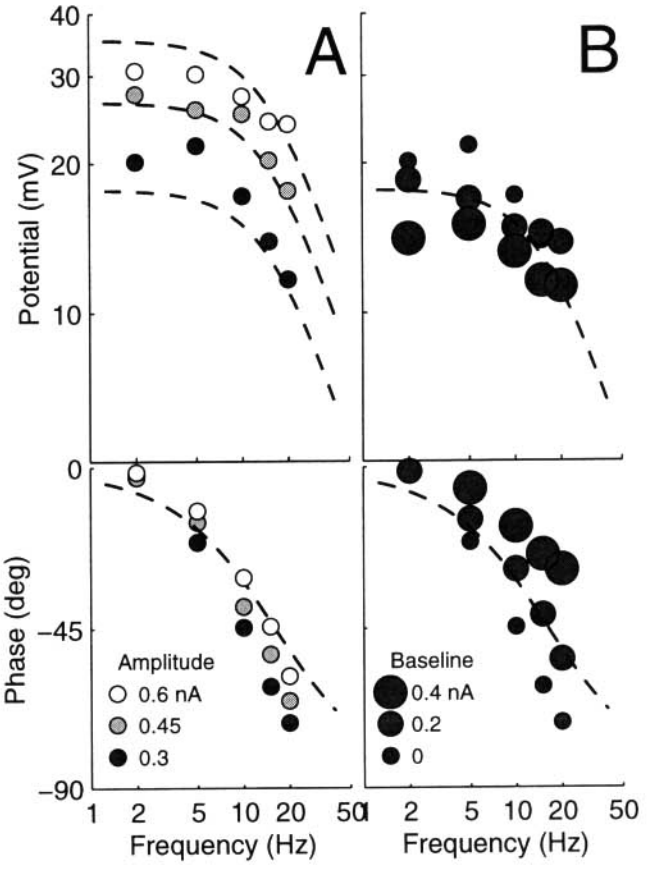

FIG. 7. Frequency tuning of the membrane potential responses to sinusoidal currents for different stimulus amplitudes (*A*) and baseline intensities (*B*). *Top*: amplitudes of the responses. *Bottom*: phases. Responses were measured by computing the first harmonic components of the membrane potential traces. The cell acted as a low-pass filter. By contrast, the firing rate responses of the same cell to the same stimuli were more band pass (Fig. 2). Dashed curves: predictions of a single-compartment passive model of the membrane, composed of a resistor and a capacitor in parallel RC circuit (*Eq. 1*). *Cell 19s2, experiment 5.*

TABLE 1. *General properties of cells in our sample*

Cell	Layer	V_{rest}, mV	R, MΩ	τ, ms
02s2	?	−56.6	28.1	8.5
02s3	?	−53.0 ± 1.6	48.4 ± 7.8	6.7 ± 1.3
05s1	III	−77.0 ± 1.4	34.5 ± 2.4	8.0 ± 1.3
15s1	II/III	−95.8 ± 3.8	109 ± 14	5.6 ± 0.6
16s1	IV/V	−70.9 ± 1.4	71.3 ± 16	17.6 ± 3.1
18s1	II/III	−76.0 ± 1.3	40.9 ± 7.9	7.1 ± 1.4
19s1	III/IV	−78.6 ± 0.1	52.3 ± 12	9.5 ± 2.4
19s2	IV/V	−70.7 ± 1.4	58.3 ± 3.5	9.3 ± 0.5
20s1	IV/V	−53.6 ± 0.5	73.4 ± 9.0	8.9 ± 1.6

Values with ± are means ± SD. V_{rest}, resting potential of the cells. Input resistance (R) and time constant (τ) were measured by fitting the frequency tuning of a single-compartment passive model of the cell membrane (*Eq. 1*) to the first harmonic of the membrane potentials obtained with sinusoidal stimulation. Large SD values indicate that the parameters varied substantially during a recording session, presumably an effect of the decaying quality of the impalements.

The third stage is a high-pass linear filter. Its output F is described in the Fourier domain by

$$\hat{F}(f) = \hat{m}(f)[1 - g_H/(1 + 2\pi i f \tau_H)] \quad (3)$$

where m is the output of the rectification stage, and g_H and τ_H are free parameters that determine the shape of the transfer function.

The model also includes a fourth stage, a half-rectifier that ensures that the predicted firing rates are positive. This stage requires no parameters. Its output is the firing rate $R(t)$ predicted by the model

$$R(t) = \max [0, F(t)]. \quad (4)$$

Figure 10, *B–E*, illustrates the output of the different stages for four different input currents. The current in *B* is a low-frequency sinusoid. The membrane potential response (V) predicted by the RC model of the membrane is quite large, and a substantial portion of it (m) is above threshold and is input to the high-pass filter. The filter enhances the portions of its input that vary rapidly in time and suppresses the portions that are roughly constant. Its rectified output (R) is thus concentrated in the upward-going portion of the sinusoidal input. The input current in Fig. 10*C* is a high-frequency sinusoid. It is substantially attenuated by the first low-pass filter, so no portion of it reaches threshold. As a consequence, the output of the model is zero. The input current in Fig. 10*D* is the sum of the ones in *B* and *C*. The output V of the first linear filter is thus the sum of its outputs in *B* and *C*. The two sinusoids help each other get across the threshold, and the output m of the rectification stage contains both the low and the high frequency. The high-pass filter enhances the high-frequency components of the input current, so the firing rate R has strong high-frequency components. The current in Fig. 10*E* is a square wave. The output V of the first linear filter is a smoothed version of the current. A substantial portion of it is above threshold, so it appears in the output m of the rectification stage. The high-pass filter enhances the initial transient and suppresses the subsequent constant portion, yielding a rapidly adapting firing rate R.

The model provided good fits to our data. For broadband noise experiments (which included eight sinusoid stimuli and eight broadband stimuli) it accounted for 78–95% of the variance of the responses (median: 89%). The percentage of the variance was measured as the variance of the difference between predicted and actual responses, divided by the variance of the actual responses. Before this measurement both responses were smoothed with a cutoff of 150 Hz. The values of the parameters obtained for each cell are listed in Table 2; the median values of the parameters were used to draw Fig. 10*A*. Figures 11–13 illustrate the fits to the data set that we have previously used when comparing the responses to broadband noise with those to single sinusoids. Because the model accounted for 86% of the variance of the responses in this data set, these figures give a conservative example of the quality of the fits.

Figure 11, *bottom*, illustrates how the sandwich model captures general features of the responses, such as the fact that the spikes are preferentially located on the rising phase of the sinusoidal currents. The thick curves are the actual firing rates of the cell, obtained by smoothing the spike trains, and the thin curves are the predictions of the model.

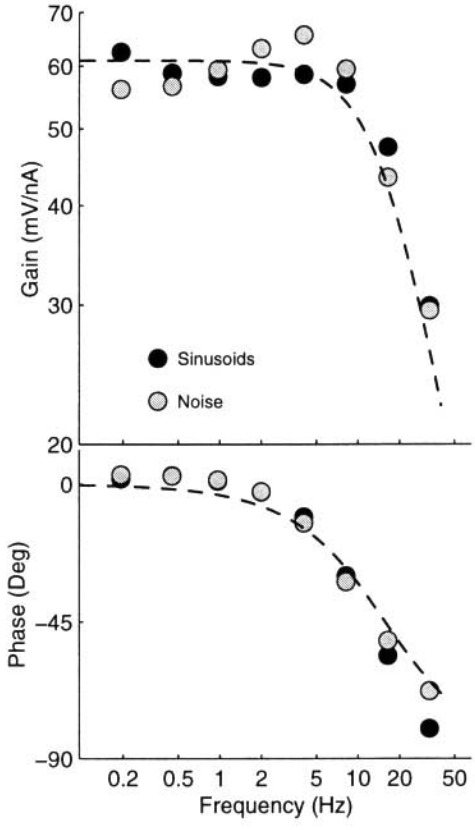

FIG. 8. Comparison of the frequency tuning of the membrane potential responses to sinusoids and to broadband noise. *Top*: gain of the responses (the membrane impedance). *Bottom*: phase. Gain was measured by computing the first harmonic of the membrane potential responses at a given component frequency and dividing the result by the intensity of that component in the stimulus. The similarity of the tuning to sinusoids and broadband noise is consistent with the cell operating as a linear system. By contrast, the firing rate responses of the same cell to the same stimuli show a substantial difference between the sinusoid and broadband noise conditions (Fig. 3). Dashed curves: fit of the single-compartment passive model of the membrane (RC circuit) to the sinusoid data. *Cell 19s2, experiment 4.*

The model predicts the locations of the clusters of spikes in response to the broadband stimuli, although it does not always predict the right number of spikes in the clusters. Another aspect of the responses that is captured by the model is the phenomenon of linearization by noise. We observed this by averaging the predicted firing rate responses over one period of a sinusoid composing the stimulus, as was done for the actual firing rate in Fig. 5. The result was much more sinusoidal when the stimulus was broadband noise than when it was a sinusoid. As pointed out by Spekreijse and Oosting (1970), linearization by noise is a general property of models that include a static nonlinearity such as the rectification stage.

To better compare the predictions of the model with the data, we performed on the simulated responses the same analysis that we had performed on the actual responses of the cells. An example of the results is shown in Fig. 12. The figure shows a comparison of the linear responses of the cell and of the model to sinusoid and broadband noise stimuli. The model correctly predicts the band-pass tuning of the responses to sinusoids, and the broadening of the tuning caused by stimulation with broadband noise. In addition, the model captures the different response phases obtained with the two kinds of stimuli, correctly predicting the lower integration time and phase lead that are obtained with the broadband stimulus.

We further evaluated the quality of the fits by analyzing the second-order kernels of the broadband noise responses, which measure the frequency component of a response at the sums and differences of frequencies present in the input (Victor and Shapley 1980; Victor et al. 1977). The second-order kernel of a response R is defined as $K_2(f_a, \pm f_b) = \hat{R}(f_a \pm f_b)$, where f_a and f_b are frequencies present in the input, and $\hat{R}(f)$ is the Fourier transform of the response R at the frequency f. Because our broadband stimuli contain eight different frequencies, K_2 assumes $2 \times 8 \times 8$ values, except that it is undefined in the eight cases in which $f_a = -f_b$.

Figure 13*A* shows the second-order kernel of the broadband noise responses of a cell. It is about half the size of the first-order kernel for the same experiment, which we illustrated in Fig. 12 (*gray* ○). For a linear system the second-order kernel is zero because all the power is concentrated at the input frequencies. In very nonlinear systems such as Y ganglion cells in the cat retina, the second-order kernels can be much larger than the first-order kernels (Victor et al. 1977).

The second-order kernel of the responses predicted by the sandwich model is shown in Fig. 13*B*. The model replicates the size, the phase, and the general shape of the second-order kernel of the actual responses. It however consistently underestimates the highest frequency components, which are shown in the far edges of the surface plots. This underestimation was present in most fits, and was in some cases evident already in the first-order kernel. Indeed, in Fig. 12 the 33-Hz component of the broadband noise response (rightmost gray data point) is underestimated by the model. For frequencies below ~30 Hz, the model provided good fits to the second-order kernels of all our cells.

Figure 14 compares the model predictions with the responses of two cells to sinusoidal currents of different amplitudes and baselines. The model captures the general behavior of the data: it predicts the dependence of the frequency tuning on the stimulus amplitude and baseline intensity. The quality of some of the fits to the sinusoid data, however, is not entirely satisfactory. An analysis of these errors shows that the model inherits the shortcomings of its first stage, the RC model of the cell's membrane. For example, the sandwich model underestimated the responses to the low-amplitude stimuli (dark symbols) in *C*. This underestimation can be traced back to the RC model underestimating the membrane potential responses to those stimuli (Fig. 7*A*). When the RC model provided good fits to the membrane potential data, as in Fig. 8, the sandwich model provided good fits to the firing rate data (Fig. 12).

To measure the degree to which the RC model of the membrane contributed to the total error in the fits, we explored the effects of bypassing it and feeding the rest of the model directly with the linear membrane potential responses

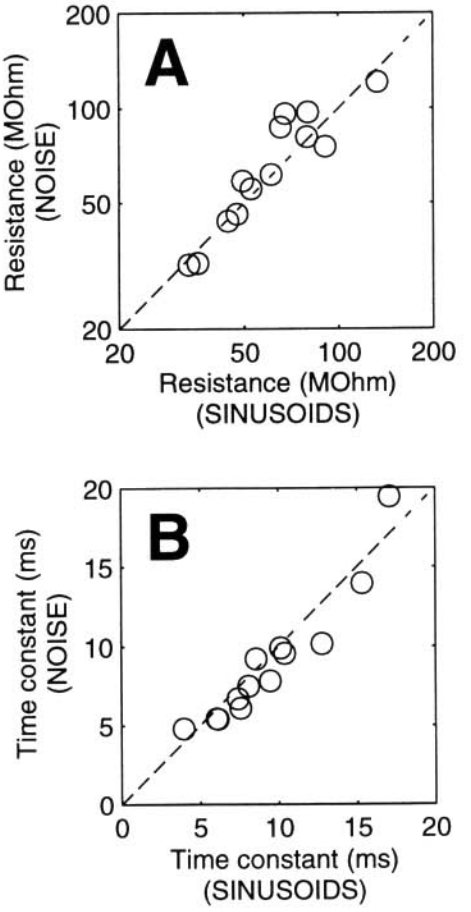

FIG. 9. Summary of the passive properties of the membrane, as measured with sinusoids (abscissae) and with broadband noise (ordinates). *A*: membrane resistance. *B*: membrane time constant. The values were obtained by fitting the broadband noise responses and the sinusoid responses with the predictions of a single-compartment passive model of the membrane. Each data point corresponds to an experiment in which sinusoid and broadband stimuli were randomly interleaved. Of the 9 cells in our sample, 4 were tested with 2 different sets of frequencies, yielding a total of 13 data points. The substantial identity of the fitted values suggests that the cells encode the input currents into membrane potentials in a linear fashion.

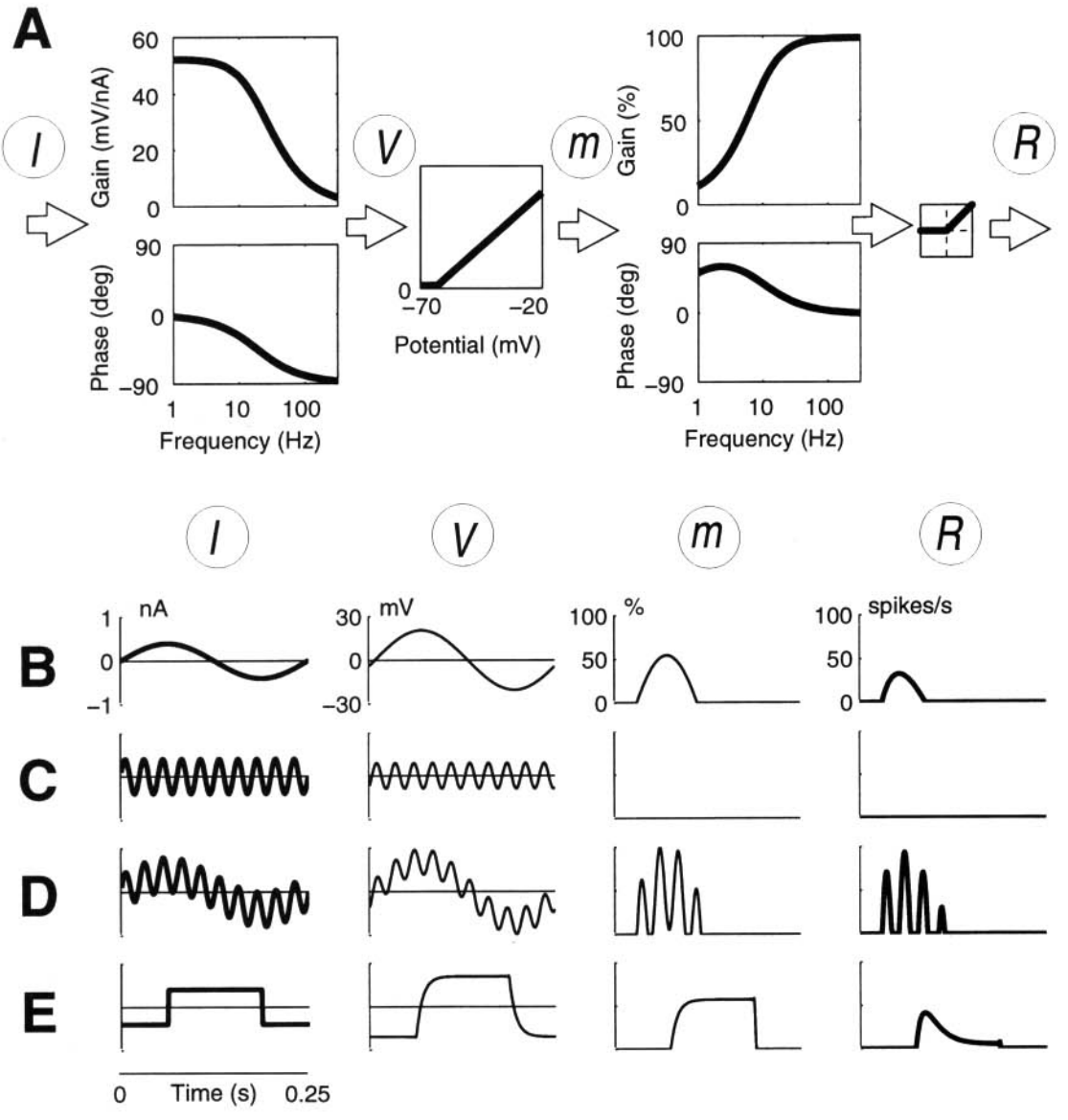

FIG. 10. Sandwich model. *A*: structure of the model. The 1st stage is a low-pass filter (the RC model of the membrane). Its inputs are the injected currents, and its outputs are the passive membrane potential responses. The 2nd stage is rectification. Its output is the amount of activation of the cell. The 3rd stage is a high-pass linear filter. Its output is fed to a (parameter-free) rectification stage, which ensures that the predicted firing rates are positive. *B–E*: output of the different stages for different input currents: a low-frequency sinusoid (*B*), a high-frequency sinusoid (*C*), the sum of the two (*D*), and a step (*E*). The model parameters used in this figure are the median values of the parameters estimated for our population (Table 2).

of the cell such as that depicted in Fig. 6*B*. Without its first stage the sandwich model becomes a model of the transformation of the "slow" membrane potential responses into firing rates similar to that proposed by Korenberg et al. (1989) for the catfish retina. The reduced model provided better fits to the spike data than the full sandwich model: whereas the fit of the full model shown in Fig. 14, *C* and *D*, accounted for 69% of the variance of the spike data, the reduced model (not shown in the figure) accounted for 84% of the variance. As a model of the transformation of the injected currents into spike trains, however, the reduced model does not constitute a good alternative to the sandwich model, because it requires knowledge of the first harmonic of the membrane potential responses to all the frequencies present in the stimulus.

A final example of the performance of the sandwich model is illustrated in Fig. 15. Figure 15, *bottom,* shows the responses of a cell to two current steps of different intensity. The thick traces show the smoothed spike trains, and the thin traces show the predictions of the sandwich model. The model exhibits spike rate adaptation because the step onset has strong high-frequency components, which are amplified by the high-pass filter much more than the subsequent constant current injection.

TABLE 2. *Parameters of sandwich model for our sample*

Cell	V_T, mV	G, spikes·s^{-1}·mV^{-1}	g_H, %	τH, ms
02s2	−49.5	107.01	98	3.2
02s3	−48.7 ± 0.0	19.0 ± 9.9	97 ± 2	57.8 ± 60
05s1	−60.0 ± 3.0	21.4 ± 19.3	88 ± 5	17.1 ± 7.7
15s1	−79.2 ± 4.4	3.0 ± 1.2	85 ± 12	43.9 ± 9.3
16s1	−61.9 ± 2.6	7.7 ± 3.0	94 ± 3	14.6 ± 7.8
18s1	−52.3 ± 4.8	7.7 ± 5.3	88 ± 14	48.3 ± 46
19s1	−56.3 ± 4.9	5.7 ± 1.8	96 ± 5	32.1 ± 8.4
19s2	−60.1 ± 1.6	7.3 ± 0.7	94 ± 4	15.3 ± 2.4
20s1	−43.8 ± 2.4	8.2 ± 2.4	84 ± 4	16.3 ± 8.9

Values with ± are means ± SD. The model was fit independently to each experiment. The first 2 parameters determine the rectification stage (*Eq. 2*): V_T, is the threshold; G, gain. The last 2 parameters determine the high-pass filter (*Eq. 3*): g_H, 0-frequency attenuation; τ_H, low-cut frequency.

DISCUSSION

The goal of this study was to gain insight into the spike-encoding properties of regular-spiking cells. To this end, we measured the spike responses of the cells to injected currents with different waveforms. We found that the spike encoder had markedly band pass properties when measured with sinusoids, and was instead not selective for stimulus frequency when measured with broadband noise, which enhanced its responsivity both to the low and to the high frequencies. In addition to enhancing the cells' responsivity, broadband noise also linearized their averaged spike responses, which were otherwise quite nonlinear.

Nonlinearities in the spike train responses

The most evident type of nonlinearity that we encountered in the spike train responses was rectification. Rectification is to be expected in cortical cells because their low resting firing rate does not allow them to encode negative currents. By contrast, some noncortical neurons that have high resting firing rates can act as linear encoders (du Lac and Lisberger 1995).

The other type of nonlinearity that we observed is spike synchronization. This nonlinearity has been observed in a variety of neural systems. These include cockroach mechanoreceptors (French et al. 1972), and eccentric cells of the *Limulus* eye (Ascoli et al. 1974). Knight (1972) observed that spike synchronization seriously limits the amount of information that a spike train can carry and showed that spike synchronization is predicted by a model of spike train generation as simple as the leaky integrate-and-fire model. On the basis of this model, Knight concluded that even very low amounts of noise should be sufficient to get rid of spike synchronization in the averaged spike train responses. This prediction was confirmed experimentally by French et al. (1972) in studies of the spike-encoding properties of a cockroach mechanoreceptor, and we have seen that it is also correct for regular-spiking cells in the visual cortex. Many other results of the present study can be likened to results

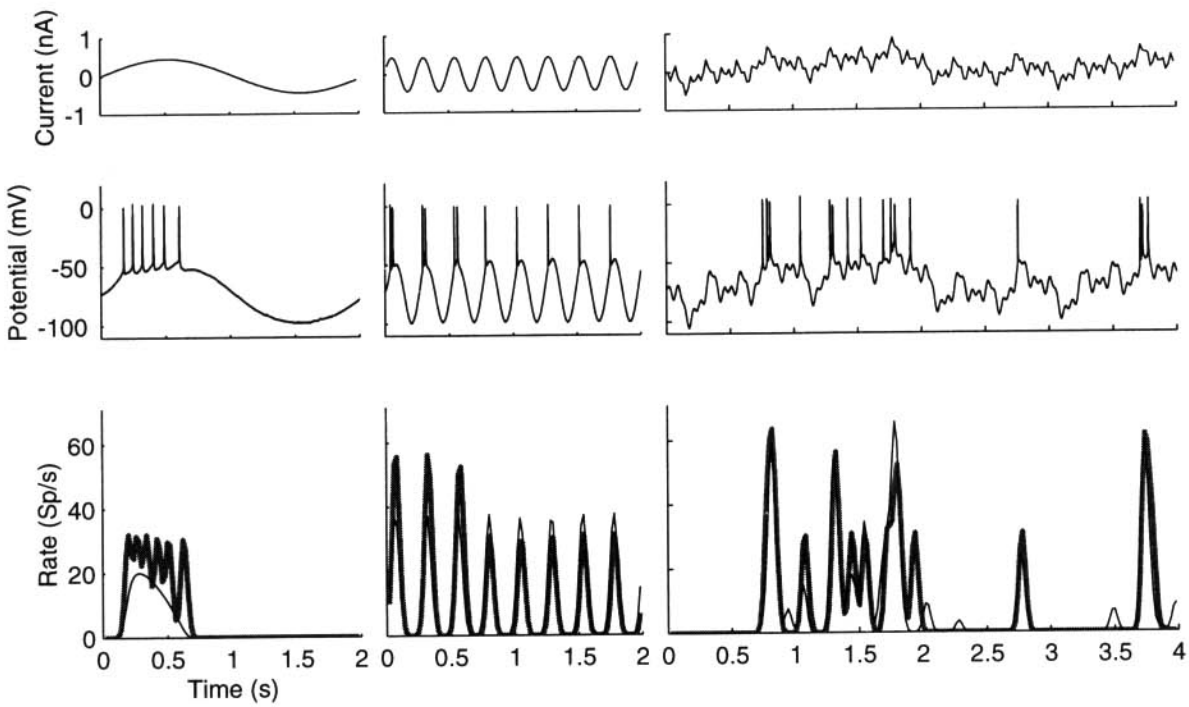

FIG. 11. Responses to a low-frequency sinusoid, to a high-frequency sinusoid, and to a broadband noise stimulus. *Top*: injected currents. *Middle*: membrane potential responses. *Bottom*: spike train responses (thick gray curves) and predictions of the sandwich model (thin black curves), both low passed by convolving with a Gaussian (σ = 25 Hz). The parameters of the sandwich model were obtained by fitting all the responses in the experiment, which consisted of 8 sinusoid stimuli and 8 broadband stimuli obtained by adding the sinusoids with 8 different sets of relative phases. *Cell 19s2, experiment 4.*

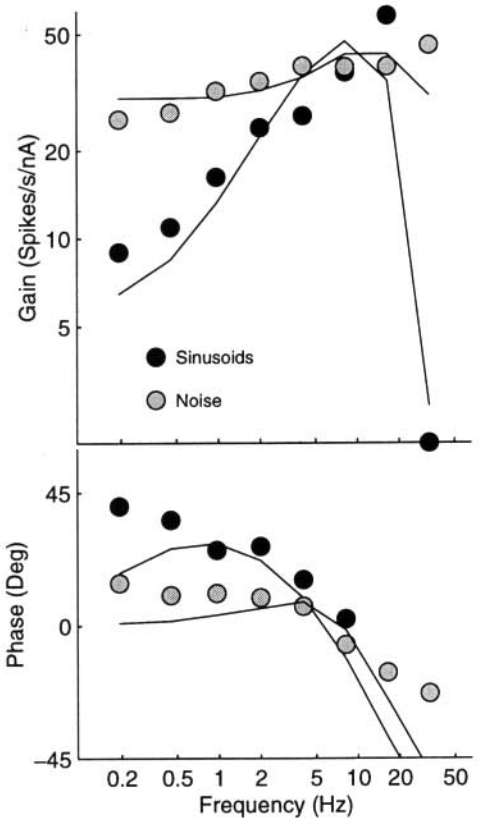

FIG. 12. Comparison of the first harmonic of the spike responses of a cell to sinusoids and broadband noise with the predictions of the sandwich model. Lines: first harmonics of the responses predicted by the sandwich model. The model predicts the enhancement in responsivity observed with broadband stimulation. It also predicts the effects of broadband stimulation on response timing: the shortening of the integration time and of the phase lead. Data points are the same as in Fig. 3. Some of the raw responses are shown in Fig. 11. *Cell 19s2, experiment 4.*

obtained in the cockroach mechanoreceptors and *Limulus* eccentric cells. For example, the frequency tunings of both types of cells measured with sinusoidal stimulation were found to be markedly band pass (French et al. 1972; Knight et al. 1970).

The sandwich model

To account for the spike responses, we used a sandwich model consisting of a low-pass linear filter (the RC circuit), a rectification nonlinearity, and a high-pass linear filter. Sandwich models have been successfully used for a variety of neural systems. Spekreijse (1969) used a sandwich model to predict the spike responses of ganglion cells in the goldfish retina to light stimulation, and Victor and Shapley (Victor 1988; Victor et al. 1977) applied it to Y ganglion cells in the cat retina. Korenberg et al. (1989) used a sandwich model to describe the generator potential responses of catfish retinal ganglion cells to light stimulation. In addition, they used a static nonlinearity followed by a band-pass linear filter to describe the transformation of generator potentials into spike trains. More directly related to this study is the work of French and Korenberg (1989), who used a sandwich model to describe the transformation of injected currents into spike trains by cockroach mechanoreceptors. Our results confirm the validity of such a model, and extend it to a different type of neuron.

A major difference between our approach and the aforementioned studies lies in our effort to limit the number of free parameters to a bare minimum. This was motivated by our goal of eventually incorporating the sandwich model into large-scale models of the visual cortex. For this reason we imposed severe restrictions on the stages of the model. In particular, we required that the first stage be a single-compartment passive model of the cell membrane (RC model). Such a model is defined by two parameters, the gain and the time constant of the membrane. We also required that the static nonlinearity be a simple rectifier, which is also described by two parameters, i.e., the threshold and the gain. Finally, we required that the second linear filter be high-pass with a very strict functional form (*Eq. 3*), also described by two parameters.

The first stage of the model—the RC model of the membrane—is the only one we can directly relate to the cell biophysics. Its parameters are derived from the membrane potential responses of the cells. By contrast, the rectification stage has no firm biophysical interpretation. It embodies a threshold that was in general lower than the voltage threshold at which spikes were generated. We think of its output as a measure of sodium channel activation. Finally, the high-pass filter can be interpreted as a phenomenological description of the effects on the spike train of sodium inactivation and of the afterhyperpolarization currents present in cortical cells.

The sandwich model captures most of the essential properties of the firing rate responses of regular-spiking cells in the visual cortex to sinusoidal stimuli, broadband noise, and step currents. In particular, the model predicts the approximately linear dependence of the firing rate on the injected current observed by Jagadeesh et al. (1992). If a stimulus is suprathreshold, increasing its amplitude results in a proportional increase in the predicted firing rate of the cells. According to the model, the slope of the current-rate line is a function of the stimulus frequency, the absolute value of the product of the two filters' transfer functions. Other properties of the spike-encoding mechanism that are captured by the model include spike rate adaptation, band-pass tuning and rectification in the responses to sinusoids, the general shape and size of the second order kernels, and the phenomenon of linearization by noise observed with broadband stimulation.

The model, however, outputs analog firing rate traces, so it cannot predict spike synchronization and other phenomena related to the exact timing of the individual spikes. Another shortcoming of the model is that it relies on a very simplified model of the membrane potential responses, the RC model, which tends to be less accurate when the injected currents have large modulations or baseline intensities. The advantage of the RC model, however, is that it is specified by only two parameters.

It would be interesting to test the sandwich model on the data of Stafstrom et al. (1984b), who measured the firing rate responses of cortical cells to current ramps. In that study, the authors discuss—and ultimately reject—a model in which the firing rate R is a weighted sum of the membrane

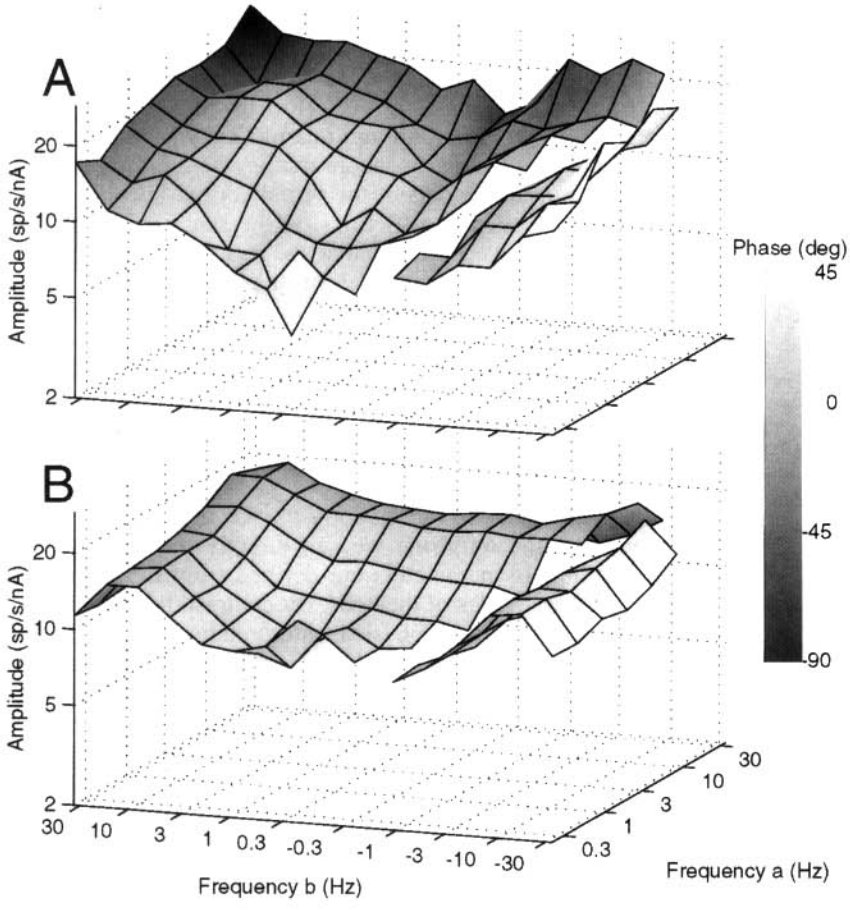

FIG. 13. Second-order kernels of the responses to broadband noise stimuli. *A*: observed. *B*: predicted by sandwich model. At each pair of frequencies f_a, f_b the 2nd-order kernel $K_2(f_a, f_b)$ is given by the component of the response at the frequency $f_a + f_b$. In the plots, surface height represents response amplitude, and gray level represents response phase. The surfaces are not defined in the diagonal in which $f_a = -f_b$. The "Frequency b" axis is the juxtaposition of 2 logarithmic axes, 1 for the positive frequencies and 1 for the negative frequencies. The observed and predicted 1st-order kernels for this cell are shown in Fig. 12 (gray circles and line fitting them). *Cell 19s2, experiment 4.*

potential V and of its derivative dV/dt. Such a model is a particular type of high-pass filter, so it is possible that the sandwich model, being more general, would provide better fits to those data.

Neuronal inputs and outputs

In natural conditions the input to a neuron is constituted by synaptic conductances. To what degree can somatic current injection simulate synaptic stimulation? Schwindt and Calvin (1973), and more recently Powers et al. (1992) and Powers and Binder (1995) showed that somatic injection of current into motoneurons has the same effect on the spike trains as synaptic stimulation. The spike train of the cell can thus be taken to reflect the overall synaptic current that reaches the site of spike initiation, which is located in the axon hillock (Stuart and Sakmann 1994). A similar conclusion was drawn by Ahmed et al. (1993), who reported that the net somatic input current can be estimated from the spike discharge of a neuron "by deconvolving the spike train response to visual stimuli with a suitably transformed response to somatic step current" (R. Douglas, personal communication). This is akin to considering the firing rate as the output of a linear filter whose input is the synaptic current. Above threshold, this model resembles the sandwich model.

Role in visual responses

The nonlinear nature of firing rate encoding in visual cortical neurons may contribute to the many nonlinearities of their contrast responses (reviewed in Heeger 1992a,b). The extent of this contribution can be roughly assessed by equating our current injection with the synaptic current resulting from visual contrast stimulation. It is reasonable to assume that the relation between visual contrast and synaptic current is monotonic, with higher visual contrasts resulting in larger modulations in the synaptic currents. For simple cells, in particular, this assumption has been tested intracellularly. The membrane potential responses were found to be consistent with a linear dependence of synaptic current on visual contrast (Jagadeesh et al. 1993).

Remarkably, the period histograms obtained from simple cells with sinusoidal contrast modulation look much more sinusoidal than those that we obtained with sinusoidal current injection. This must be due to the synaptic and active currents that result from sinusoidal visual stimulation containing power at many frequencies besides that of the stimulus (Jagadeesh et al. 1993). This "noise" linearizes the averaged responses, which are therefore more sinusoidal than they would have been if they had received a perfectly sinusoidal current as input.

On the basis of our results, we suggest that spike encoding may contribute to the increase in the temporal resolution of

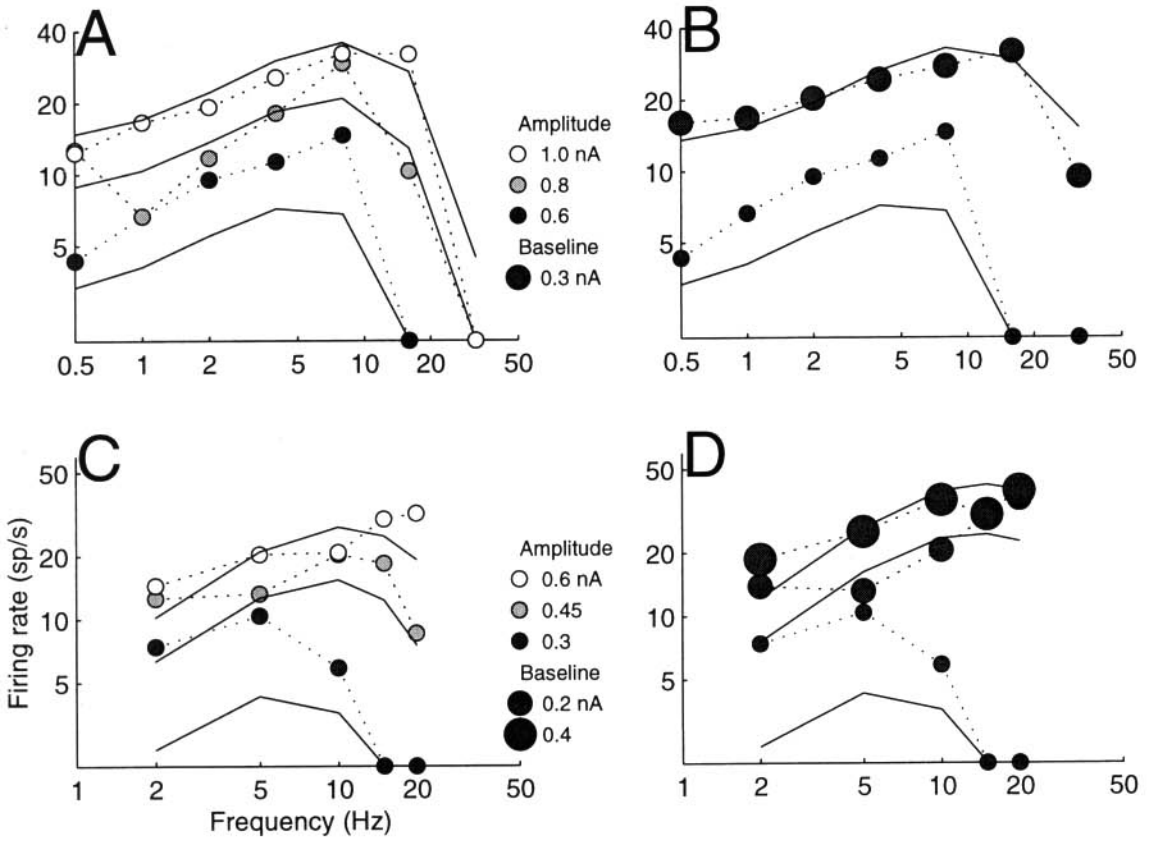

FIG. 14. Comparison of the amplitudes of the first harmonics of the spike responses of 2 cells to sinusoids with the predictions of the sandwich model. *A* and *B*: responses of a cell to sinusoids of different amplitudes and baselines. The model captures the rightward shift in the tuning curves observed with increasing amplitude or baseline. *Cell 05s1, experiment 10/6. C* and *D*: same data as in Fig. 2, fitted with the predictions of the sandwich model.

V1 cells observed with increasing visual contrasts (Hawken et al. 1992; Holub and Morton-Gibson 1981). Indeed, increasing the current amplitude in our sinusoidal current injections had a similar effect on the high-cut temporal frequency (Fig. 2*A*).

Spike encoding is also likely to contribute to the differences in the temporal frequency bandwidth and integration time observed with broadband noise and sinusoidal contrast modulations (Reid et al. 1992). The broadband stimuli used in the present study were constructed in the same way as those used by Reid et al., i.e., by adding eight different sinusoids. Similarly to Reid et al., we found that the cells were more responsive to the low and high frequencies when they were stimulated with broadband noise than when the stimuli were sinusoidal. Moreover, we found that the increase in bandwidth was accompanied by a decrease in integration time of ~10 ms. By comparison, the decrease in integration time reported by Reid et al. with visual contrast modulation is 20-30 ms. The difference in bandwidth between the sinusoid and broadband noise conditions was, however, most probably larger in our injected currents than in the synaptic and active currents resulting from visual stimulation. As a consequence, the spike encoding mechanism likely played a lesser role in the results of Reid et al. than in our experiments.

Another temporal nonlinearity in which spike encoding may play a role is the increased transiency of the responses to contrast steps with respect to the predictions from sinusoidal contrast modulation (Tolhurst et al. 1980). Indeed, the spike responses to step currents are more transient than predicted from the tuning to sinusoids: the frequency tuning deduced from the step responses showed more low-frequency attenuation than that measured with sinusoids (Carandini et al. 1995).

High frequencies and visual responses

Intracellular in vivo records of visual cortical cells show that their membrane potential contains substantial power at frequencies in the 40- to 100-Hz range (Jagadeesh et al. 1992). We have seen that if other frequencies are present in the stimulus, as is the case for our broadband stimulus, the cortical cells can encode such high-frequency signals into their spike trains. Indeed, high-frequency components have been observed in the spike responses of visual cortical cells (Gray and Singer 1989), and are considered by some to carry an important signal (Singer 1991). High-frequency signals may not be sufficiently strong to elicit spikes by themselves, but could serve to determine the timing of the spikes when larger, but more slowly varying, signals are superimposed.

Our results suggest an additional role for these high-fre-

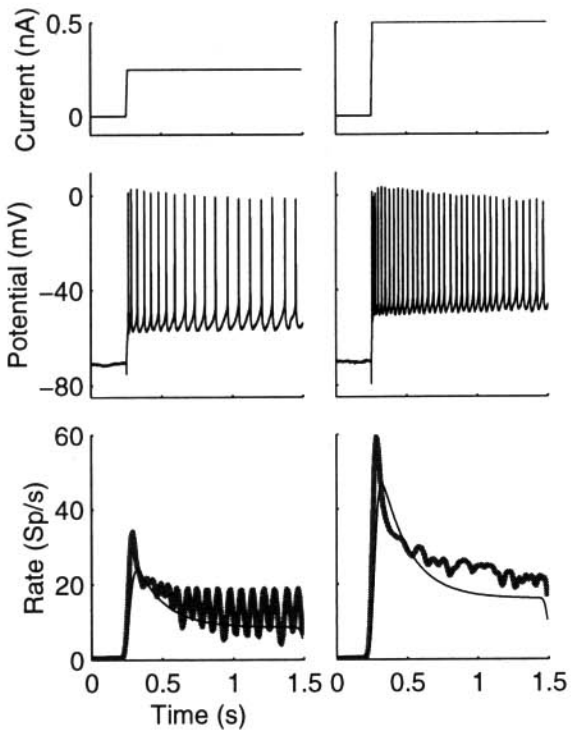

FIG. 15. Responses to current steps. *Top*: injected currents. *Middle*: membrane potential responses. *Bottom*: spike train responses (thick gray curves) and predictions of the sandwich model (thin black curves), both low passed by convolving with a Gaussian (σ = 30 Hz). The model captures the spike rate adaptation because its last stage is a high-pass filter, which attenuates the responses to steady inputs. *Cell 19s2, experiment 3.*

quency fluctuations, related to the phenomenon of linearization by noise and to the broadening of the range of encoded frequencies caused by broadband stimulation that we observed in the spike mechanism. By increasing the stimulus bandwidth, the high-frequency fluctuations can act to effectively amplify and linearize the spike responses to lower-frequency currents, improving the ability of the cells to pass information about the visual stimuli.

In conclusion, we have described the basic properties of spike encoding in a class of cortical cells. We found that the bandwidth of the signals can profoundly affect the input/output properties of the neurons. In addition, we have proposed a model that succeeds in describing the spike-encoding mechanism while using very few parameters. Our hope is that such a model will help in the interpretation of extracellularly recorded spike trains, and will improve the design of large-scale models of the cerebral cortex.

We thank M. Hawken, B. Knight, C. Koch, F. Lui, B. Shapley, D. Tranchina, and J. Victor for helpful suggestions.

This research was supported by National Institute of Neurological Disorders and Stroke Grant NS-27881 to C. S. Leonard and by a Howard Hughes Medical Institute Investigatorship to J. A. Movshon.

Present address and address for reprint requests: M. Carandini, Dept. of Neurobiology and Physiology, Northwestern University, 2153 N. Campus Drive, Evanston, IL 60208.

E-mail: matteo@nwu.edu

Received 16 April 1996; accepted in final form 10 July 1996.

REFERENCES

AHMED, B., ANDERSON, J. C., DOUGLAS, R. J., MARTIN, K. A. C., AND WHITTERIDGE, D. A method of estimating net somatic input current from the action potential discharge of neurones in the visual cortex of the anaesthetized cat (Abstract). *J. Physiol. Lond.* 459: 134, 1993.

ASCOLI, C., BARBI, M., GHELARDINI, G., AND PETRACCHI, D. Rectification and spike synchronization in the *Limulus* lateral eye. *Kybernetik* 14: 155–160, 1974.

BOWER, J. M. AND BEEMAN, D. *The Book of GENESIS.* New York: Springer-Verlag, 1995.

CARANDINI, M., MECHLER, F., LEONARD, C. S., AND MOVSHON, J. A. Firing rate encoding by visual cortical neurons in vitro. *Soc. Neurosci. Abstr.* 20: 624, 1994.

CARANDINI, M., MECHLER, F., LEONARD, C. S., AND MOVSHON, J. A. Spike rate encoding can explain some visual properties of cortical cells (Abstract). *Invest. Opthalmol. Visual Sci.* 36: S692, 1995.

CHOUDHURY, B. P. Retinotopic organization of the guinea pig's visual cortex. *Brain Res.* 144: 19–29, 1978.

COLE, K. S. AND BAKER, R. F. Longitudinal impedance of the squid giant axon. *J. Gen. Physiol.* 24: 771–788, 1941.

CONNORS, B. W. AND GUTNICK, M. J. Intrinsic firing patterns of neocortical neurons. *Trends Neurosci.* 13: 99–104, 1990.

CONNORS, B. W., GUTNICK, M. J., AND PRINCE, D. A. Electrophysiological properties of neocortical neurons in vitro. *J. Neurophysiol.* 48: 1302–1320, 1982.

CREEL, D. J. AND GIOLLI, R. A. Reticulogeniculate projections in the guinea pigs: albino and pigmented strains compared. *Exp. Neurol.* 36: 411–425, 1972.

DOUGLAS, R. J. AND MARTIN, K. A. Neocortex. In: *The Synaptic Organization of the Brain,* edited by G. M. Shepherd. Oxford, UK: Oxford Univ. Press, 1990, p. 389–438.

FRENCH, A. S., HOLDEN, A. V., AND STEIN, R. B. The estimation of the frequency response function of a mechanoreceptor. *Kybernetik* 11: 15–23, 1972.

FRENCH, A. S. AND KORENBERG, M. J. A nonlinear cascade model for action potential encoding in an insect sensory neuron. *Biophys. J.* 55: 655–661, 1989.

GETTING, P. A. Reconstruction of small neural networks. In: *Methods in Neuronal Modeling,* edited by C. Koch and I. Segev. Cambridge, MA: MIT Press, 1989, p. 171–194.

GRAY, C. M. AND SINGER, W. Stimulus-specific neuronal oscillations in orientation columns of cat visual cortex. *Proc. Natl. Acad. Sci. USA* 86: 1698–1702, 1989.

GUTFREUND, Y., YAROM, Y., AND SEGEV, I. Subthreshold oscillations and resonant frequency in guinea-pig cortical neurons: physiology and modelling. *J. Physiol. Lond.* 483: 621–640, 1995.

GUTNICK, M. J. AND CRILL, W. E. The cortical neuron as an electrophysiological unit. In: *The Cortical Neuron,* edited by M. J. Gutnick and I. Mody. Oxford, UK: Oxford Univ. Press, 1995 p. 33–51.

HAWKEN, M. J., SHAPLEY, R. M., AND GROSOF, D. H. Temporal frequency tuning of neurons in macaque V1: effects of luminance contrast and chromaticity (Abstract). *Invest. Opthalmol. Visual Sci. Suppl.* 33: 955, 1992.

HEEGER, D. J. Normalization of cell responses in cat striate cortex. *Visual Neurosci.* 9: 181–198, 1992a.

HEEGER, D. J. Half-squaring in responses of cat simple cells. *Visual Neurosci.* 9: 427–443, 1992b.

HODGKIN, A. L. AND HUXLEY, A. F. A quantitative description of membrane current and its application to conduction and excitation in nerve. *J. Physiol. Lond.* 117: 500–544, 1952.

HOLUB, R. A. AND MORTON-GIBSON, M. Response of visual cortical neurons of the cat to moving sinusoidal gratings: response-contrast functions and spatiotemporal interactions. *J. Neurophysiol.* 46: 1244–1259, 1981.

JAGADEESH, B., GRAY, C. M., AND FERSTER, D. Visually evoked oscillations of membrane potential in cells of cat visual cortex. *Science Wash. DC* 257: 552–554, 1992.

JAGADEESH, B., WHEAT, H. S., AND FERSTER, D. Linearity of summation of synaptic potentials underlying direction selectivity in simple cells of the cat visual cortex. *Science Wash. DC* 262: 1901–1904, 1993.

KNIGHT, B. W. Dynamics of encoding in a population of neurons. *J. Gen. Physiol.* 59: 734–766, 1972.

KNIGHT, B. W., TOYODA, J., AND DODGE, F. A. A quantitative description

of the dynamics of excitation and inhibition in the eye of *Limulus*. *J. Gen. Physiol.* 56: 421–437, 1970.

KOCH, C. Cable theory in neurons with active, linearized membranes. *Biol. Cybern.* 50: 15–33, 1984.

KOCH, C. AND SEGEV, I. *Methods in Neuronal Modeling*. Cambridge, MA: MIT Press, 1989.

KORENBERG, M. J., SAKAI, H. M., AND NAKA, K. Dissection of the neuron network in the catfish inner retina. III. Interpretation of spike kernels. *J. Neurophysiol.* 61: 1110–1120, 1989.

DU LAC, S. AND LISBERGER, S. G. Cellular processing of temporal information in medial vestibular nucleus neurons. *J. Neurosci.* 15: 8000–8010, 1995.

LLINÀS, R. R., GRACE, A. A., AND YAROM, Y. In vitro neurons in mammalian cortical layer 4 exhibit intrinsic oscillatory activity in the 10- to 50-hz frequency range. *Proc. Natl. Acad. Sci. USA* 88: 897–901, 1991.

LORENZON, N. M. AND FOEHRING, R. C. Relationship between repetitive firing and after-hyperpolarizations in human neocortical neurons. *J. Neurophysiol.* 67: 350–363, 1992.

MCCORMICK, D. A., CONNORS, B. W., LIGHTHALL, J. W., AND PRINCE, D. A. Comparative electrophysiology of pyramidal and sparsely spiny stellate neurons of the neocortex. *J. Neurophysiol.* 54: 782–806, 1985.

MCCORMICK, D. A. AND HUGUENARD, J. R. A model of the electrophysiological properties of thalamocortical relay neurons. *J. Neurophysiol.* 68: 1384–1400, 1992.

MOVSHON, J. A., THOMPSON, I. D., AND TOLHURST, D. J. Receptive field organization of complex cells in the cat's striate cortex. *J. Physiol. Lond.* 283: 79–99, 1978.

POWERS, R. K. AND BINDER, M. D. Effective synaptic current and motoneuron firing rate modulation. *J. Neurophysiol.* 74: 793–801, 1995.

POWERS, R. K., ROBINSON, F. R., KONODI, M. A., AND BINDER, M. D. Effective synaptic current can be estimated from measurements of neuronal discharge. *J. Neurophysiol.* 68: 964–968, 1992.

REID, R. C., VICTOR, J. D., AND SHAPLEY, R. M. Broadband temporal stimuli decrease the integration time of neurons in cat striate cortex. *Visual Neurosci.* 9: 39–45, 1992.

SCHWINDT, P. C. AND CALVIN, W. H. Equivalence of synaptic and injected current in determining the membrane potential trajectory during motoneuron rythmic firing. *Brain Res.* 59: 389–394, 1973.

SCHWINDT, P. C., SPAIN, W. J., AND CRILL, W. E. Influence of anomalous rectifier activation on afterhyperpolarizations of neurons from cat sensorimotor cortex in vitro. *J. Neurophysiol.* 59: 468–481, 1988a.

SCHWINDT, P. C., SPAIN, W. J., FOEHRING, R. C., CHUBB, M. C., AND CRILL, W. E. Slow conductances in neurons from cat sensorimotor cortex in vitro and their role in slow excitability changes. *J. Neurophysiol.* 59: 450–467, 1988b.

SCHWINDT, P. C., SPAIN, W. J., FOEHRING, R. C., STAFSTROM, C. E., CHUBB, M. C., AND CRILL, W. E. Multiple potassium conductances and their functions in neurons from cat sensorimotor cortex in vitro. *J. Neurophysiol.* 59: 424–449, 1988c.

SILVA, L. R., AMITAI, Y., AND CONNORS, B. W. Intrinsic oscillations of neocortex generated by layer 5 pyramidal neurons. *Science Wash. DC* 251: 432–435, 1991.

SINGER, W. The formation of cooperative cell assemblies in the visual cortex. In: *Neuronal Cooperativity*, edited by J. Krüger. Berlin: Springer-Verlag, 1991, p. 165–183.

SPATZ, W. B., VOGT, D. M., AND ILLING, R. B. Delineation of the striate cortex and the striate-peristriate projections in the guinea pig. *Exp. Brain Res.* 84: 495–504, 1991.

SPEKREIJSE, H. Rectification in the goldfish retina: analysis by sinusoidal and auxiliary stimulation. *Vision Res.* 9: 1461–1472, 1969.

SPEKREIJSE, H. AND OOSTING, H. Linearizing: a method for analysing and synthesizing nonlinear systems. *Kybernetik* 7: 1461–1472, 1970.

STAFSTROM, C. E., SCHWINDT, P. C., AND CRILL, W. E. Properties of subthreshold response and action potential recorded in layer V neurons from cat sensorimotor cortex in vitro. *J. Neurophysiol.* 52: 244–263, 1984a.

STAFSTROM, C. E., SCHWINDT, P. C., AND CRILL, W. E. Repetitive firing in layer V neurons from cat neocortex in vitro. *J. Neurophysiol.* 52: 264–277, 1984b.

STAFSTROM, C. E., SCHWINDT, P. C., AND CRILL, W. E. Cable properties of layer V neurons from cat sensorimotor cortex in vitro. *J. Neurophysiol.* 52: 278–288, 1984c.

STUART, G. J. AND SAKMANN, B. Active propagation of somatic action potentials into neocortical pyramidal cell dendrites. *Nature Lond.* 367: 69–72, 1994.

SUAREZ, H. H., KOCH, C., AND DOUGLAS, R. J. Modeling direction selectivity of simple cells in striate visual cortex within the framework of the canonical microcircuit. *J. Neurosci.* 15: 6700–6719, 1995.

TOLHURST, D. J., WALKER, N. S., THOMPSON, I. D., AND DEAN, A. F. Nonlinearities of temporal summation in neurones in area 17 of the cat. *Exp. Brain Res.* 38: 431–435, 1980.

VICTOR, J. The dynamics of the cat retinal Y cell subunit. *J. Physiol. Lond.* 405: 289–320, 1988.

VICTOR, J. AND SHAPLEY, R. M. A method of nonlinear analysis in the frequency domain. *Biophys. J.* 29: 459–484, 1980.

VICTOR, J., SHAPLEY, R. M., AND KNIGHT, B. W. Nonlinear analysis of cat retinal ganglion cells in the frequency domain. *Proc. Natl. Acad. Sci. USA* 74: 3068–3072, 1977.

VICTOR, J. D. AND KNIGHT, B. W. Nonlinear analysis with an arbitrary stimulus ensemble. *Q. Appl. Math.* 37: 113–136, 1979.

WREE, A., ZILLES, K., AND SCHLEICHER, A. A quantitative approach to cytoarchitectonics. VII. The areal pattern of the cortex in the guinea pig. *Anat. Embryol.* 162: 81–103, 1981.